Static and Dynamical Properties of Polystyrene in *trans*-Decalin. 1. NBS 705 Standard Near Θ Conditions‡

T. Nose† and B. Chu*

Chemistry Department, State University of New York at Stony Brook, Long Island, New York 11794. *Received January 11, 1979*

ABSTRACT: Static and dynamical properties, in terms of the osmotic compressibility, the diffusion coefficient, and the frictional coefficient of polystyrene (NBS 705 standard, $\bar{M}_w$ = 179 300, $\bar{M}_w/\bar{M}_n$ = 1.07) in *trans*-decalin, have been studied from dilute to concentrated polymer concentrations of 0.346 g/g of solution at and up to 20 °C above the Θ temperature by means of laser light scattering. Although traces of simple power law relations can be established, we observe gradual changes of osmotic compressibility as a function of concentration. Our experiments using polymers of finite molecular weight suggest that the limiting simple power laws need to be modified for application to polymer solutions under realistic conditions and that we should not take the power law exponents seriously except at limiting conditions. By means of a histogram method of data analysis, we have established the presence of an additional gel-like mode which is faster than the hydrodynamic mode. The large variance in line width can be explained by the presence of this bimodal line width distribution.

Static and dynamical properties of polymers in solution in the semidilute and gel regions have been of recent interest partly because of the success of new theoretical tools in the application of scaling theories and the renormalization-group technique to the more concentrated polymer solution and partly because of recent advances in small-angle neutron-scattering experiments, such as deuterium labeling and position sensitive detectors, and in light-scattering spectroscopy which permits crucial tests on both the static and dynamical properties of polymers in solution in regions where coils overlap and networks form. The scaling theories[1-9] proposed by de Gennes are based upon an analogy with critical phenomena in magnetic systems. Kosmas and Freed[10] have presented a derivation of a scaling theory of the thermodynamics of polymer solutions at finite concentrations. Adler and Freed[11] have derived dynamical scaling relations for the diffusion coefficient, viscosity, and dynamic structure factor for polymer chains at infinite dilution.

The small-angle neutron scattering of polystyrene ($\bar{M}_w$ = 1.14 × 10^3 and 5 × 10^5) in carbon disulfide[3,12] (a good solvent) has shown the following results in the semidilute regime where polymer chains overlap strongly, but the solvent fraction is still large: (a) the radius of gyration $r_g(C)$ for one deuterated chain in a solution of normal chains where concentration C obeys the relation $\langle r_g^2(C)\rangle \sim C^{-0.25\pm0.02}$; (b) the screening (or correlation or coherence) length ξ which represents the characteristic length of the concentration correlation function $\langle C(r_1)C(r_2)\rangle$ is proportional to $C^{-0.72\pm0.06}$; and (c) the osmotic compressibility $\chi(C)$ is proportional to $C^{-1.25\pm0.04}$. These results are different from the predictions of the mean field theory, which are: r_g independent of C, $\xi \sim C^{-1/2}$, and $\chi \sim C^{-1}$. The dynamical behavior of polystyrene ($\bar{M}_w$ varying from 2.4 × 10^4 to 2.4 × 10^7) in benzene (a good solvent) has been reported by Adam and Delsanti.[13] They determined three dynamical exponents, α, β, and γ: (a) in dilute solution, the hydrodynamic radius r_h is proportional to M with α = 0.55 ± 0.02 in the molecular weight range 2.4 × 10^4 to 3.8 × 10^6, while the geometrical radius scales as M^ν with ν = 0.6; (b) the cooperative diffusion coefficient D_c is proportional to C^{β^*} with β^* = 0.67 ± 0.02 in the semidilute region where polymer chains overlap; and (c) in dilute solution, at wave vector $K > r_g^{-1}$ ($Kr_g \geq 4.4$), the inverse characteristic time[14] $\tau^{-1}(K)$ is proportional to K^γ with γ = 2.85 ± 0.05. K [=$(4\pi/\lambda)\sin(\theta/2)$] is the magnitude of the momentum transfer vector with λ and θ being the wavelength of light in the medium and the scattering angle, respectively. Adam and Delsanti further indicated that the exponents could be connected by scaling laws: $\alpha = (3\nu - 1)\beta^*$, $\gamma = 2 + \alpha/\nu$.

The static[4,5] and dynamical[15,16] behavior of semidilute polymer solutions in Θ conditions has also been reported. Daoud and Jannink[4] explored a temperature–concentration diagram of polymer solutions by identifying the polymer Θ point with the tricritical point accessible at infinite molecular weight and infinite dilution and predictions have subsequently been confirmed partially by neutron-scattering experiments of polystyrene in cyclohexane[5] with $\xi \propto C^{-1}$ at the Θ temperature in the semidilute region. In a Θ solvent, the polymer coil tends to contract and to form more knots on itself, while in a good solvent, the chain expands and makes but few knots on itself. Thus, in a Θ solvent in the semidilute region, the dynamical property of polymer coils must be dominated by the hydrodynamic mode in which the polymer diffuses as a whole. The elastic modulus associated with this mode, E_0, varies as C^3 is varied. Coupled with the hydrodynamic mode, there exists also a weaker gel mode whose spectral width is proportional to K^2 at sufficiently large values of K; the elastic modulus corresponding to the gel mode, E_{gel}, varies as C^2 is varied. Observation of the gellike concentration fluctuation modes by light-scattering spectroscopy has been difficult due to the presence of a range of relaxation modes giving rise to nonexponential behavior.[17,18] Following the earlier work of Tanaka, Hocker, and Benedek,[19] Geissler and Hecht[16] reported photon correlation spectroscopy measurements of the collective motion diffusion coefficient D_{gel} and the longitudinal elastic modulus E_{gel} of poly(acrylamide) gels in the poor solvent region using a water–methanol (3–1 by volume) mixture as solvent. By using *N,N'*-methylenebis(acrylamide) (bis) as a cross-linking agent and bis–acrylamide (B–A) ratios of 1–75, they tried to trap the slower movement of uncrossed-linked branches and the relaxation of self-entanglements without causing a precipitation and clouding in the gel. The resultant line width Γ_{gel} was proportional to K^2 and $E_{gel} = C(\partial\pi/\partial C) \sim C^{3.07\pm0.07}$ for C between 0.07 and 0.3 g/cm^3 in the semidilute (gel) region. The power law dependence of D_{gel}, however, is accidental, since ξ and the "solvent" viscosity η_0 are concentration dependent.

There is no doubt that the scaling theories of polymer solutions represent a major advance in the understanding of concentrated polymer solution behavior. The relations,

‡ Work supported by the National Science Foundation.

† On leave of absence from the Department of Polymer Chemistry, Tokyo Institute of Technology, Tokyo, Japan.

0024-9297/79/2212-0590$01.00/0

in terms of simple power laws, emerge from asymptotic dimensional analysis for infinitely long chains. In a manner analogous to the critical-point studies, the simple power laws are valid only asymptotically in the immediate neighborhood of the critical point. For example, we[20] have established that the value of the asymptotic critical exponent β of a polymer solution (polystyrene with $\bar{M}_w = 1.56 \times 10^6$ in cyclohexane) is like that calculated for the Ising model provided that we use extended scaling.[21] Thus, at finite concentrations and at finite molecular weight and temperature, the limiting simple scaling relations can predict only approximate polymer solution behavior. Although simple scaling relations are valid only in regions not easily accessible by experiments, we believe that further refinements, such as those analogous to extended scaling in critical phenomena studies, but not necessarily in the same formalism, should be extremely valuable in providing a practical general polymer solution theory at finite concentrations. As all polymer solutions have similar phase behavior,[4,22,23] and even poly(acrylamide)gels exhibit a spinodal temperature,[24,25] we have selected for the present study a NBS 705 standard polystyrene in a Θ solvent (*trans*-decalin). By choosing a relatively low molecular weight ($\bar{M}_w$ = 179 300) polymer and by using a Θ solvent where the polymer coil tends to contract under Θ conditions, we have avoided studying the internal segmental motions of the polymer coil and emphasized the Gaussian coil behavior. In this article, we wish to show an analysis of our light-scattering intensity and line width measurements indicating the approximate nature of simple scaling theories for a polymer of finite molecular weight. In the next section, we shall outline the theoretical expressions used in our measurements. In the following three sections, we shall describe the experimental procedures, the methods of data analysis, and the results and discussion of this study, respectively.

Theoretical Background[45]

1. Dilute Region. a. Static Properties. In the osmotic compressibility, $(\partial \pi/\partial C^v)_{T,P}$, we compute

$$(\partial \pi/\partial C^v)_{T,P} = H\,(\partial n/\partial C^v)_{T,P}{}^2 C^v RT/R_c(0) \qquad (1)$$

from the excess Rayleigh ratio $R_c(0)$ due to concentration fluctuations obtained from absolute excess scattered intensity extrapolated to zero scattering angle and H $4\pi^2 n^2/(N_A \lambda_0{}^4)$, with n, C^v, N_A, T, P, and R being the refractive index of the solution, the polymer concentration in g/cm^3, the Avogadro number, the absolute temperature, the pressure, and the gas constant, respectively.

In dilute solution, the virial expansion has the form

$$(\partial \pi/\partial C^v)_{T,P} = RT/\bar{M}_w + 2A_2 RTC^v + \ldots \qquad (2)$$

where A_2 is the second virial coefficient. At infinite dilution, $(\partial \pi/\partial C^v)_{T,P} = RT/\bar{M}_w$. We shall define the Θ temperature to be that at $A_2 = 0$ when M is infinitely large. For our sample, $\bar{M}_w$ = 179 300, the temperature at which $A_2 = 0$ should be approximately equal to the Θ temperature. At finite scattering angles and finite concentrations in the dilute solution region, eq 1 has a modified form:

$$\frac{HC^v}{R_c(C^v,K)} = \left(\frac{1}{\bar{M}_w} + 2A_2C^v\right)\left(1 + (1 + 2A_2C^v\bar{M}_w)^{-1}\frac{\langle r_g{}^2(C^v)\rangle_z}{3}K^2\right) \qquad (3)$$

or in terms of $\sin^2 \theta/2$, we have

$$\frac{HC^v}{R_c(C^v,\theta)} = \frac{1}{\bar{M}_w}\left(1 + \frac{16\pi^2 n^2}{3\lambda_0{}^2}\langle r_g{}^2(C^v)\rangle_z \sin^2(\theta/2)\right) + 2A_2C^v \qquad (4)$$

Thus, in a plot of $HC^v/R_c(C^v,\theta)$ vs. $\sin^2(\theta/2)$,

$$\langle r_g{}^2(C^v)\rangle_z = \frac{\text{initial slope}}{\text{intercept}}(1 + 2A_2C^v\bar{M}_w)\frac{3\lambda_0{}^2}{16\pi^2 n^2} \qquad (5)$$

The terms A_2 and $\bar{M}_w$ can be determined from a plot of

$$\lim_{\theta\to 0}\frac{HC^v}{R_c(C^v)} \text{ vs. } C^v$$

where we have

$$\lim_{\theta\to 0}\frac{HC^v}{R_c(C^v)} = \frac{1}{\bar{M}_w} + 2A_2C^v \qquad (6)$$

We have defined the apparent radius of gyration as

$$\langle r_g{}^2(C^v)\rangle_z{}^* = \langle r_g{}^2(C^v)\rangle_z/(1 + 2A_2C^v\bar{M}_w) \qquad (7)$$

b. Dynamical Properties. The translational diffusion coefficient for dilute polymer solutions can be expanded to first order in concentration as

$$D = D_0(1 + k_D C^v + \ldots) \qquad (8)$$

where D_0 ($=k_BT/f_0$) is the diffusion coefficient at infinite dilution, with k_B and f_0 denoting the Boltzmann constant and the frictional coefficient at infinite dilution. $D = \Gamma/K^2$ and is defined by eq 29 for a polydisperse sample. The hydrodynamic and thermodynamic factors are combined in k_D as[45]

$$k_D = 2A_2M - k_f - N_AV_1/M \qquad (9)$$

where k_f is the first-order friction coefficient, and $\bar{v}$ ($=N_AV_1/M$) is the specific volume of the polymer with V_1 being the polymer molecular volume. At finite concentrations, the corresponding frictional coefficient has the form:

$$f = f_0(1 + k_fC^v + \ldots) \qquad (10)$$

where $f_0 = 6\pi\eta_0 r_h$ and the equivalent hydrodynamic radius $r_h = k_BT/6\pi\eta_0 D_0$ with η_0 being the solvent viscosity. $C^v = C\rho_s$ where ρ_s is the solvent density. In a plot of f/η_0 vs. C, we get

$$r_h = \text{intercept}/6\pi \qquad (11)$$

and

$$k_f + \bar{v} = \frac{\text{initial slope}}{\text{intercept}}\rho_s \qquad (12)$$

At the Θ temperature, $A_2 = 0$, and

$$k_D{}^\Theta = -(k_f + \bar{v}) \qquad (13)$$

where $k_f = N_AV_h/M$ according to the Yamakawa[26] and Imai[27] (Y, I) theories and $k_f = 2.23N_AV_h/M$ according to the Pyun and Fixman (PF) theory[28] with V_h ($=4\pi r_h{}^3/3$) being the hydrodynamic volume of the polymer molecule. At temperatures higher than the Θ temperature, we have

$$k_f = 1.2A_2M + N_AV_h/M \qquad \text{(Y, I)} \qquad (14)$$

in the nondraining limit and

$$k_f = (7.16 - K^*(A^*))N_AV_h/M \qquad \text{(PF)} \qquad (15)$$

where $A^* = 2n_s{}^2v_\beta/8\pi r_h{}^3$ with n_s and v_β being the number of segments per polymer coil and the excluded volume between two segments, respectively.

According to the Pyun and Fixman theory, we need to evaluate A^* and then $K^*(A^*)$ before k_f can be computed.

Although perturbation theory[29,30] yields

$$\alpha_s^2 = 1 + 1.276Z - 2.082Z^2 + \ldots \quad (16)$$

$$A_2 = (N_A n_s^2 v_\beta / 2M^2)(1 - 2.865Z + 14.278Z^2 - \ldots) \quad (17)$$

for small values of Z, eq 17 for A_2 is not a good approximation to small variations of Z in the experimental range $|Z| \leq 0.19$ which we encounter here. Thus, we used a modified FKO equation:[31]

$$A_2 = (N_A n_s^2 v_\beta / 2M^2) \frac{\ln (1 + 5.73\bar{Z})}{5.73\bar{Z}} \quad (18)$$

where $\bar{Z} = Z/\alpha_s^3$, $Z = n_s^2 v_\beta (4\pi \langle r_g^2 \rangle_0)^{-3/2}$, and $\alpha_s = \langle r_g^2 \rangle^{1/2} / \langle r_g^2 \rangle_0^{1/2}$, with $\langle r_g^2 \rangle_0^{1/2}$ being the radius of gyration in the absence of long-range interactions. At the Θ temperature, $\langle r_g^2 \rangle_0^{1/2} = \langle r_g^2 \rangle_{T=\Theta}^{1/2}$. We find $n_s^2 v_\beta$ and Z from A_2 by means of eq 16 and 18, compute A^* then $K^*(A^*)$, and finally compute k_f from eq 15.

2. Semidilute and Gel Regions. a. Static Properties. At finite concentrations where polymer coils overlap, eq 1 remains valid even though the physical interpretation for $(\partial \pi / \partial C^v)_{T,P}$ can be quite different, e.g., the quantity can be related to the longitudinal elastic modulus of polymer gels. In the dilute region, $(\partial \pi / \partial C)_{T,P} \sim C^{\sim 0}$; in the semidilute region, $(\partial \pi / \partial C)_{T,P} \sim C^{5/4}$; and in the concentrated solution (gel) region, $(\partial \pi / \partial C)_{T,P} \sim C^2$.

b. Dynamical Properties. We can write down a general expression for the macroscopic diffusion coefficient:

$$D = \frac{C^v}{f} \left(\frac{\partial \mu}{\partial C^v} \right)_{T,P} \quad (19)$$

where the chemical potential can be related to the osmotic compressibility

$$C^v (\partial \mu / \partial C^v)_{T,P} = \frac{(1 - \bar{v} C^v) M}{N_A} (\partial \pi / \partial C^v)_{T,P} \quad (20)$$

By combining eq 19 and 20, the frictional coefficient at finite concentrations can be expressed as

$$f = \frac{M(1 - \bar{v} C^v)}{D N_A} (\partial \pi / \partial C^v)_{T,P} \quad (21)$$

Equations 19 and 21 are valid at high concentrations. However, the physical interpretations can again become complex in the semidilute and gel regions because the implicit assumption of identifying $\bar{\Gamma}/K^2$, as defined by eq 29, with only the macroscopic diffusion coefficient in the hydrodynamic mode, may break down.

Experimental Procedures

1. Sample Preparation. Polystyrene (NBS 705 standard, $M_w = 179\,300$, $M_w/M_n = 1.07$) was dissolved in benzene and then freeze-dried in vacuum. *trans*-Decalin (Tokyo Kasei Kogyo Co. Ltd.) was dried in $CaCl_2$ anhydride, passed through a silica gel column (1.5 cm o.d. × 80 cm), and then fractionally distilled under partial vacuum (~15 mmHg) at 70–75 °C in a helium atmosphere using a Perkin-Elmer Model 251 autoannular still. The purified *trans*-decalin contains less than 1% impurity (mainly the cis content) when analyzed by gas chromatography. All solutions were prepared under dry helium atmosphere. We first made a 7 wt % polymer solution, and it was filtered through a Millipore filter of nominal pore diameter of 0.22 μm. Solutions at lower concentrations were prepared by dilution of a known amount of the filtered stock solution directly in the light-scattering cell using filtered purified *trans*-decalin. Those at higher concentrations were prepared by evaporation of the solvent from a known amount of the filtered stock solution in the light-scattering cell using a mild vacuum. All cells containing solutions of desired concentrations were subsequently flame sealed while the solutions (in vacuum) were cooled by dry ice–methanol. By the above method of preparation, we were able to cover a concentration range of 0.2 to ~35 wt % for light-scattering studies.

2. Apparatus. The detailed design of the light-scattering spectrometer has been described elsewhere.[32,33] In the present experiment, we used an argon ion laser (Coherent Radiation Model 54) operating at 488.0 nm and ~100 mW. The single-clipped photoelectron count autocorrelation function was measured using a 96-channel Malvern correlator. Temperature was controlled to ±0.02 °C and measured to 0.01 °C. Intensity was measured separately using an Ortec Model 715 dual counter which permits ratio measurements of scattered intensity/laser intensity. Thus, fluctuations of the incident light intensity were automatically compensated.

We used benzene as a reference for computing the Rayleigh ratio R_c and took $R_{vv}^B(\theta = 90°) = 3.26 \times 10^{-5}$ cm^{-1} for vertically polarized incident and scattered light at $\lambda_0 = 488.0$ nm and 30 °C.[33] With

$$(R_{vv}^B)_t = (R_{vv}^B)_{25}(1 + 0.368 \times 10^{-2}(t - 25\ °C)) \quad (22)$$

where t is temperature expressed in °C,[34] we obtained $(R_{vv}^B)_{25} = 3.20 \times 10^{-5}$ cm^{-1}. In view of the high concentrations, we have also examined the effect of attenuation on the measured scattered intensity I_{meas} which has been reduced due to the turbidity τ with $I_{meas} = I_s e^{-\tau d}$, where d is the light path length. In our case, $\tau d \ll 1$ and $\xi K < 1$, τ could be estimated by integrating I_{meas} over all scattering angles with

$$I_s = I_{meas}(1 + \pi^2 R(\phi = 90°, \theta = 0°) d) \quad (23)$$

where θ and ϕ are respectively the scattering angle and the azimuthal angle. In the present experiment, we found $I_s/I_{meas} < 1.03$ even for the strongest scattering solutions studied.

The refractive index of *trans*-decalin at $\lambda_0 = 488.0$ nm was estimated to be 1.47521, 1.47081, and 1.46641 at 20, 30, and 40 °C, respectively. dn/dC at $\lambda_0 = 488.0$ nm and different temperatures was calculated according to an expression proposed by Outer, Carr, and Zimm:[35]

$$dn/dC = 0.581 - (n_0 - 1)/\rho_2 \quad (24)$$

where ρ_2 is the density of the polymer with $\rho_2 = 1.05$ and 1.04 g/cm^3 at 20 and 30 °C, respectively.

Methods of Data Analysis

The measured single-clipped photocount autocorrelation function for a detector of finite effective photocathode has the form:

$$G_k^{(2)}(\tau) = A(1 + \beta |g^{(1)}(\tau)|^2) \quad (25)$$

where $g^{(1)}(\tau)$ is the normalized correlation function of the scattered electric field, k is the clipping level, A is the background, and β is an unknown parameter in the data-fitting procedure. τ ($=I\Delta\tau$) is the delay time with I and $\Delta\tau$ being the channel number and the increment delay time, respectively.

For a polydisperse sample with a continuous distribution of sizes and in the absence of internal motions, or for a system exhibiting a distribution of collective motions which can be represented by a superposition of exponential decays, $g^{(1)}(\tau)$ has the form:

$$|g^{(1)}(\tau)| = \int_0^\infty G(\Gamma) \exp(-\Gamma\tau)\, d\Gamma \quad (26)$$

where $G(\Gamma)$ is the normalized distribution of decay rates.

Two methods of data analysis were used: (1) cumulants method and (2) histogram method.

1. Cumulants Method.[36] Only limited information is available in terms of an average line width $\bar{\Gamma}$ and its variance $\mu_2/\bar{\Gamma}^2$ where

$$\bar{\Gamma} = \int G(\Gamma)\Gamma\, d\Gamma \quad (27)$$

$$\mu_i = \int (\Gamma - \bar{\Gamma})^i G(\Gamma)\, d\Gamma \quad (28)$$

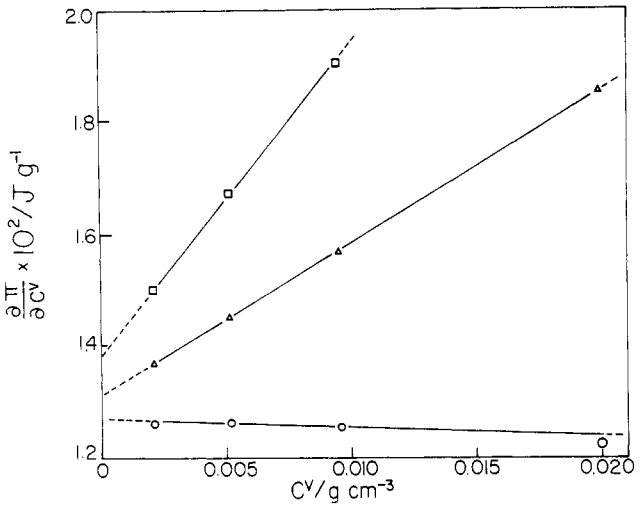

Figure 1. Plots of $\partial \pi/\partial C^v$ vs. C^v at 40 °C (hollow squares), 30 °C (hollow triangles), and 20 °C (hollow circles) for polystyrene (NBS 705 standard) in *trans*-decalin. Note: Same polymer and solvent for all subsequent figures.

Higher order moments, e.g., beyond the third moment (μ_3), cannot be determined easily. Nevertheless, when $Kr_g \ll 1$, we have a z-average translational diffusion coefficient in the dilute region and similar weighting factors for the collective motions so long as $K\xi \ll 1$,

$$\bar{D} = \bar{\Gamma}/K^2 = \sum_i C_i M_i D_i / \sum_i C_i M_i \qquad (29)$$

and $\mu_2/\bar{\Gamma}^2$ $(=\overline{D^2} - \bar{D}^2)/\bar{D}^2)$ is the normalized z-average variance of the distribution function.

2. Histogram Method.[37] We approximate $G(\Gamma)$ by means of a histogram such that

$$|g^{(1)}(\tau)| = \sum_{j=1}^{n} G(\Gamma_j) \int_{\Gamma_j - \Delta\Gamma/2}^{\Gamma_j + \Delta\Gamma/2} \exp(-\Gamma I \Delta\tau)\, d\Gamma \qquad (30)$$

where $G(\Gamma_j)$ is the total integrated scattered intensity contributing to the amplitude of the Γ_j increment from $\Gamma_j - \Delta\Gamma/2$ to $\Gamma_j + \Delta\Gamma/2$, n is the number of steps in the histogram, and $\Delta\Gamma$ $[=(\Gamma_{max} - \Gamma_{min})/n]$ is the width of each step with Γ_{max} and Γ_{min} signaling the stop and start of the range of the histogram. The normalization condition for $G(\Gamma)$ has been defined by the condition

$$\sum_{j=1}^{n} G(\Gamma_j)\Delta\Gamma = 1 \qquad (31)$$

The values of $G(\Gamma_j)$ were obtained by the method of nonlinear least squares where we minimize χ^2 with respect to each a_j simultaneously,

$$\frac{\partial}{\partial a_j}\chi^2 = \frac{\partial}{\partial a_j}\sum\left\{\frac{1}{\sigma_I^2}[Y_m(I\Delta\tau) - Y(I\Delta\tau)]^2\right\} = 0 \qquad (32)$$

where $a_j \equiv G(\Gamma_j)$, $Y(I\Delta\tau) = A\beta|g^{(1)}(I\Delta\tau)|^2$, and σ_I represents the uncertainty of data point $Y_m(I\Delta\tau)$ with the subscript m denoting the measured value. We have not yet made extensive analysis of our line width data by the recently developed histogram method. Only initial findings by the histogram analysis will be included in this article.

Results and Discussion

1. Dilute Region. a. Static Properties. We extrapolated the excess absolute scattered intensity to zero scattering angle in order to obtain $R_c(C^v,0)$. $(\partial \pi/\partial C^v)_{T,P}$ was computed according to eq 1 using n, $\partial n/\partial C^v$ and $R_c(0)$. Figure 1 shows plots of $\partial \pi/\partial C^v$ vs. C^v at 20, 30, and 40 °C. The straight line behavior clearly confirms eq 2 with

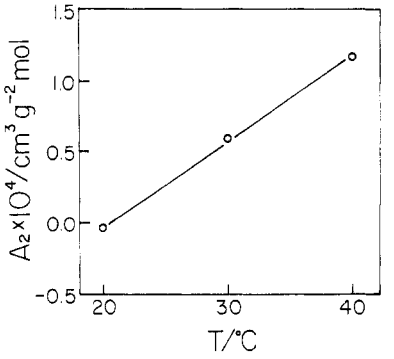

Figure 2. Plot of the second virial coefficient A_2 vs. temperature. The Θ temperature was ≈ 20.5 °C, the temperature at which $A_2 = 0$, even though M_w = 179 300, is not infinite.

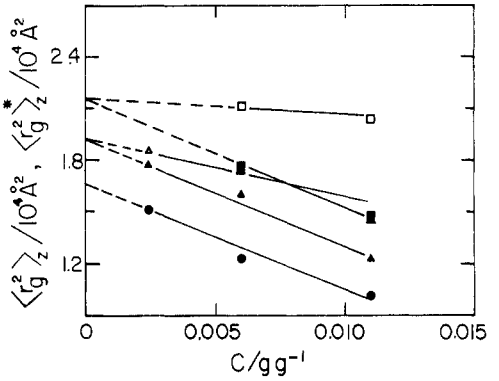

Figure 3. Plots of $\langle r_g^2(C^v)\rangle_z$ and $\langle r_g^2(C^v)\rangle_z^*$ vs. C at 20, 30, and 40 °C [t, °C, symbol for $\langle r_g^2(C^v)\rangle_z$ (eq 5), and symbol for $\langle r_g^2(C^v)\rangle_z^*$ (eq (7))]: 20, ○, ●; 30, △, ▲; and 40, □, ■. At 20 °C, $A_2 \approx 0$. Therefore, $\langle r_g^2\rangle_z \approx \langle r_g^2\rangle_z^*$.

intercept = $RT/\bar{M}_w$ and slope = $2A_2RT$. The values of A_2 are plotted in Figure 2 as a function of temperature. Using this finite molecular weight sample, we obtained a Θ temperature at 20.5 °C, in very good agreement with the cloud-point experiments of Nakata et al.[38] It should be noted that the phase transition temperature increased markedly in the presence of only a trace amount of water.[39] Thus, the agreement between our light-scattering measurements and the cloud-point curve results, rather than the osmotic pressure experiments where the solutions were exposed to air, confirms that we have prepared our solutions properly, at least in the dilute solution region. The intercepts in Figure 3 show that we have determined the molecular weight at three different temperatures. We obtained $\bar{M}_w = 1.9 \times 10^5$, which compares favorably with the NBS result of $\bar{M}_w$ = 179 300.

Figure 3 shows plots of $\langle r_g^2(C^v)\rangle_z$ and $\langle r_g^2(C^v)\rangle_z^*$ vs. C^v at 20, 30, and 40 °C according to eq 5 and 7. We shall define $\langle r_g^2(0)\rangle_0$ as the square of the radius of gyration in the absence of long-range interactions. We shall also take $\langle r_g^2\rangle$ to be the value at infinite dilution. Although $\langle r_g^2\rangle_0 = \langle r_g^2\rangle_{T=\Theta}$ at the Θ temperature, at other temperatures $\langle r_g^2\rangle_0 \neq \langle r_g^2\rangle_{T=\Theta}$. Then, we need to write

$$\alpha_s(T) = \frac{\langle r_g^2\rangle_T^{1/2}}{\langle r_g^2\rangle_{T=\Theta}^{1/2}} \frac{\langle r_g^2\rangle_{T=\Theta}^{1/2}}{\langle r_g^2\rangle_{0,T}^{1/2}} \qquad (33)$$

where $\langle r_g^2\rangle_{0,T}/\langle r_g^2\rangle_{T=\Theta} \approx 1 + (1/\langle r_g^2\rangle_0)\,(d\langle r_g^2\rangle_0/dt)(T - \Theta)$, and from rubber elasticity studies,[40] we have $d \ln \langle r_g^2\rangle_0/dT = 0.4 \times 10^{-3}$ deg^{-1}, where T is expressed in K. The results for A_2, $\langle r_g^2\rangle$, and α_s together with α_s calculated from eq 16 and 18 are listed in Table Ia.

b. Dynamical Properties. In Rayleigh line width spectroscopy, we used the cumulants method to obtain $\bar{D}$

Table I
Polystyrene (NBS 705 Standard) in *trans*-Decalin in the Dilute Region

(a) Static Properties			
temp, °C	20	30	40
A_2, 10^{-4} (cm³ mol)/g²	−0.036	0.593	1.17
$\langle r_g^2\rangle^{1/2}$, Å	130	138	146
α_s	~1.0	1.06	1.12
α_s (based on eq 16 and 18)		1.05	1.08
(b) Dynamical Properties			
$\bar{D}_0$, 10^{-7} cm²/s	1.11	1.33	1.59
$\bar{f}/\eta_0$, 10^{-5} cm	1.72	1.77	1.82
$\bar{r}_h$, Å	91.1	93.9	96.8
k_f, cm³/g	23.0	37.5	48.5
$(\bar{M}_w k_f)/(N_A \bar{V}_h)$	2.2	3.1	3.8
$\bar{r}_h/\langle r_g^2\rangle^{1/2}$	0.70	0.68	0.66

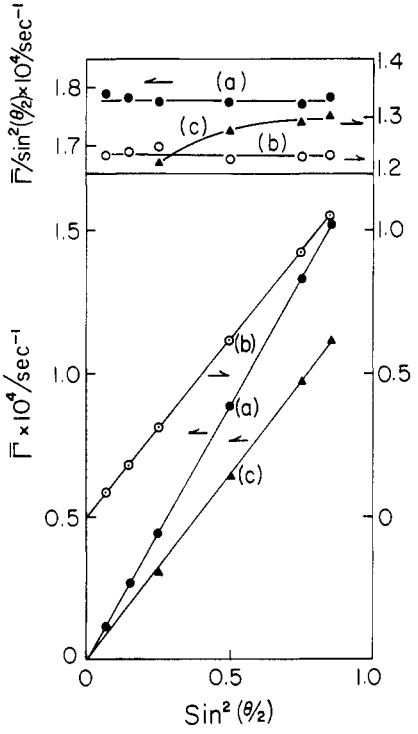

Figure 4. Plots of $\bar{\Gamma}$ vs. $\sin^2(\theta/2)$ at 30 °C: (a) dilute region, C = 0.00594 g/g of solution; (b) C = 0.165 g/g of solution; and (c) C = 0.233 g/g of solution. $\bar{\Gamma}/K^2$ is observed for C = 0.00594, 0.165, and 0.233 g/g of solution. For curve (c), the slight deviation at low scattering angles can be attributed to the dust effect.

$(=\bar{\Gamma}/K^2)$. Figure 4 shows typical plots of $\bar{\Gamma}$ versus $\sin^2(\theta/2)$ at 30 °C from dilute solutions to the concentrated solution region. In the dilute solution region, the line width distribution is mainly due to the molecular weight distribution function which gives rise to a distribution of the translational diffusion coefficient.[41]

By measuring $\bar{M}_w$, $\bar{D}$, $\bar{v}$, C^v, and $(\partial\pi/\partial C^v)_{T,P}$, we can compute $\bar{f}$ according to eq 21. In dilute solution, plots of $\bar{f}/\eta_0$ vs. C at different temperatures, as shown in Figure 5, yield r_h and $k_f + \bar{v}$ from eq 11 and 12, respectively. The results are listed in Table Ib. Figure 6 shows plots of $\bar{f}/\eta_0$ vs. temperature (°C) at different concentrations. At infinite dilution, $\bar{r}_h$ has a weak positive temperature dependence. It should be noted that the values of $r_h/\langle r_g^2\rangle^{1/2}$ are very close to the theoretical value of 0.665 according to the Kirkwood–Reiseman theory. We measured the solution at 0.00243 g/g from below the Θ temperature to 40 °C and noted an apparent linear temperature dependence of $\bar{f}/\eta_0$ over the 25 °C temperature range. Figure 7 shows a comparison of $\bar{M}_w k_f/N_A \bar{V}_h$ as a function of temperature between theory and experiment. Very near

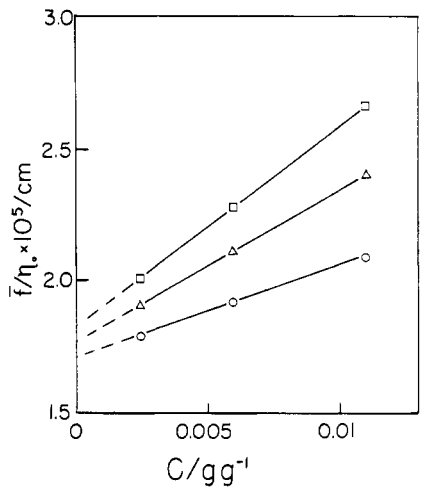

Figure 5. Plots of $\bar{f}/\eta_0$ versus C at 40 °C (hollow squares), 30 °C (hollow triangles), and 20 °C (hollow circles).

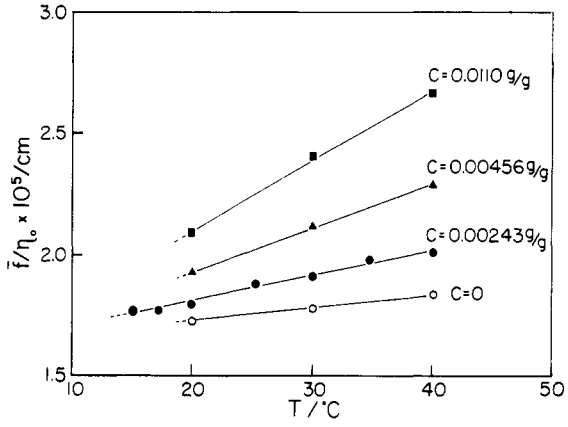

Figure 6. Plots of $\bar{f}/\eta_0$ vs. T at different concentrations.

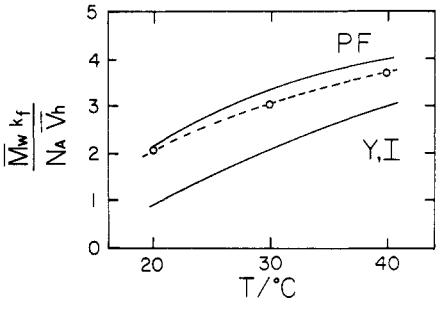

Figure 7. A comparison of $\bar{M}_w k_f/N_A \bar{V}_h$ as a function of temperature between theory and experiment: PF, Pyun and Fixman theory, eq 15; Y, I, Yamakawa and Imai theory, eq 14. Experimental values are denoted by the hollow circles.

the Θ temperature, our result is in excellent agreement with that of the PF theory which has been verified using polystyrene in cyclohexane by a previous experiment.[41] Although the agreement deteriorates with increasing temperature, the experimental values remain closer to the PF theory rather than the (Y, I) theory up to 40 °C.

2. Semidilute and Gel Regions. a. Static Properties. Figure 8 shows plots of osmotic compressibility as a function of concentration at 20, 30,[42] and 40 °C. At low concentrations in the dilute region, the behavior has been expanded in Figure 1 to show the temperature dependence of A_2. At 20 °C, A_2 has a slightly negative value as the Θ temperature is estimated to be 20.5 °C. The initial slope at 30 and 40 °C increases with increasing temperature. The transitions from dilute to semidilute and then to concentrated solutions are gradual without sharp

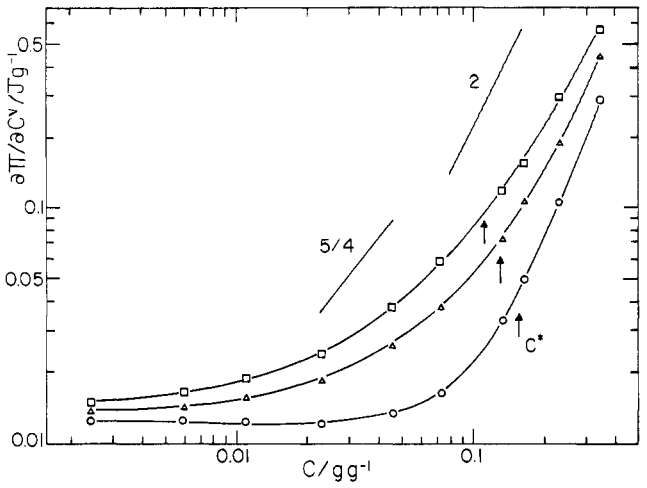

Figure 8. Plots of osmotic compressibility as a function of concentration at 40 °C (hollow squares), 30 °C (hollow triangles),[42] and 20 °C (hollow circles).

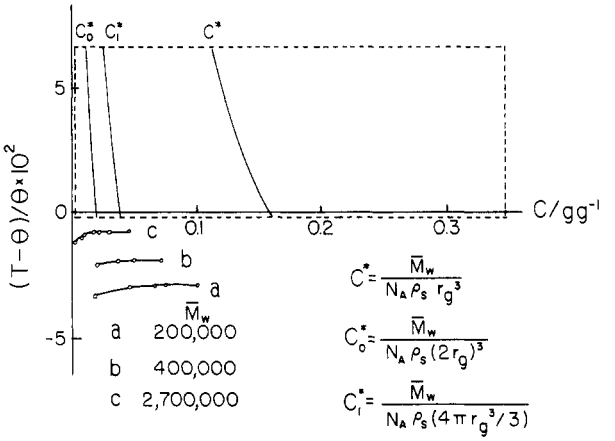

Figure 9. Temperature–concentration diagram based on experimental values of $\bar{M}_w$ and $\langle r_g^2 \rangle_z$ and the coexistence curves.[38] Θ = 20.5 °C. Note the deviations from the schematic diagram proposed in ref 4.

identifiable slope changes. If we take the overlap concentration C^* to be

$$C^* = \bar{M}_w/(N_A \rho_s \langle r_g^2 \rangle_z^{3/2}) \tag{34}$$

there are very limited regions where the $^5/_4$ exponent holds, even though qualitatively we can observe regions with $(\partial \pi/\partial C^v)_{T,P}$ proportional to $C^{\sim 0}$, $C^{5/4}$, and C^2. Furthermore, the curve at 20 °C (hollow circles) exhibits a lack of $(\partial \pi/\partial C)_{T,P} \sim C^{5/4}$ for the semidilute region. Thus, for polymers of finite molecular weight at finite concentrations, we see that the limiting simple power law behavior must be modified. Figure 9 shows a portion of the temperature–concentration diagram based on experimental values of $\bar{M}_w$ and $\langle r_g^2 \rangle_z$ and on coexistence curves.[38] The overlap concentration, though arbitrary in definition, represents a very high cross-over concentration to the semidilute region. It stretches our imagination to consider a 10 wt % polymer solution as the domain where the semidilute region emerges. Yet, as shown in Figure 8, we did observe the $^5/_4$ exponent near C^* at 30 and 40 °C even though the concentration ranges where the simple power law relations appear to hold remain very limited. We can easily define C_0^* $(=\bar{M}_w/N_A\rho_s(2r_g)^3)$ and C_1^* $(=\bar{M}_w/N_A\rho_s(4\pi r_g^3/3))$ which differ from C^* by as much as a factor of 8. For concentrations below C_0^*, we expect dilute solution behavior, even though we need to invoke higher-order virial coefficients at 40 °C as the curve is no longer

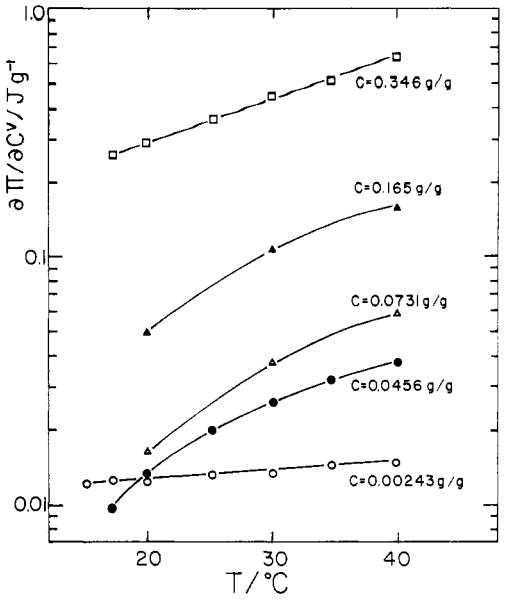

Figure 10. Plots of osmotic compressibility as a function of temperature at different fixed concentrations.

linear. At present, we are not aware of any theory which can predict this transition behavior quantitatively. In Figure 9, we see that, near the Θ temperature, there is essentially no measurable region where $\langle r_g^2 \rangle_z$ (or C^*) remains constant as a function of temperature. Figure 10 shows plots of $(\partial \pi/\partial C^v)_{T,P}$ versus temperature at different concentrations. At low concentrations in the dilute solution region (0.00243 and 0.0456 g/g of solution), we note that at temperatures greater than the Θ temperature, A_2 is positive. Therefore, $(\partial \pi/\partial C^v)_{T,P}$ at C = 0.0456 g/g of solution has a higher value than that at C = 0.00243 g/g. The two curves should essentially cross-over at the Θ temperature (20.5 °C), as shown in Figure 10. At temperatures below the Θ temperature, $(\partial \pi/\partial C^v)_{T,P}$ at C = 0.00243 g/g of solution has a higher value than that at C = 0.0456 g/g because A_2 is negative. It is important to keep in mind the experimental temperature–composition diagram of Figure 9. At increasing concentrations between 0.073 and 0.165 g/g of solution, we suggest the presence of long-range critical point effects, even though the system is not in the immediate neighborhood of the critical point. As the concentration approaches the critical solution concentration and T approaches T_c, the critical temperature, $(\partial \pi/\partial C)_{T,P} \rightarrow 0$. We can then expect to observe a sharper drop off in the osmotic compressibility with decreasing temperatures for temperatures near or below the Θ temperature. At very high concentrations (C = 0.346 g/g of solution) in the gel region, we have observed essentially a linear temperature dependence for the osmotic compressibility.

b. Dynamical Properties. In the semidilute and concentrated solution regions, we can identify a hydrodynamic mode only in the limit of very low scattering angles where $K\xi \ll 1$. At higher values of K, the $\bar{D}$ notation actually has a more complex physical meaning, even though we still observe mainly the hydrodynamic mode with a K^2 dependence. We shall refer to an analysis of the time correlation function in the semidilute-gel regions by the histogram method later. The lower $\bar{\Gamma}$ values at small scattering angles for curve (c) of Figure 4 suggest the presence of dust particles in the concentrated solution.

We checked the dust contribution by measuring the excess scattered intensity due to dust at small scattering angles and the corresponding apparent line width $\bar{\Gamma}_{app}$ due to the presence of homodyning between the scattered

Table II
Dust Contribution in a Concentrated Solution of Polystyrene in *trans*-Decalin

(a) 23.3 wt % Polystyrene; t = 30 °C

θ, [a]	60	90	135
$\Delta I/I_{app}$, [b] %	5	$\lesssim$1	<1
$\Delta\bar{\Gamma}/\bar{\Gamma}$, %	6	2	<1

(b) 34.6 wt % Polystyrene; θ = 90°

t, °C	20	40
$\Delta I/I_{app}$	7.5	17.6
$\Delta\bar{\Gamma}/\bar{\Gamma}$	~12	17.2

[a] $f^* = \Delta I/I_{app} = \Delta\bar{\Gamma}/\bar{\Gamma}$. [b] $\Delta I = I_{app} - I_s = I_d$.

intensity of polymers and that of the dust particles. If we take the intensity scattered by the dust particles to be essentially independent of temperature, we can make an estimate of the dust contribution from deviations in linear plots of I_s^{-1} vs. K^2 at different temperatures. Similarly, at low scattering angles we can observe the apparent decrease from linear plots of $\bar{\Gamma}$ vs. K^2, such as curve (c) in Figure 4.

If we take the dust particles to be fairly large, then the effective decay time due to dust ($1/\Gamma_d$) must be large or the line width Γ_d must be small. The normalized signal autocorrelation function has the form:

$$|g^{(1)}(\tau)|^2 = (1 - f^*)\exp(-2\bar{\Gamma}\tau) + 2f^* \times (1 - f^*)\exp(-(\bar{\Gamma} + \Gamma_d)\tau) + f^{*2}\exp(-2\Gamma_d\tau) \quad (35)$$

with $\bar{\Gamma} + \Gamma_d \approx \bar{\Gamma}$ and $e^{-2\Gamma_d\tau} \approx 1$, we have

$$|g^{(1)}(\tau)|^2 \approx (1 - f^*)^2\exp(-2\bar{\Gamma}\tau) + 2f^*(1 - f^*)\exp(-\bar{\Gamma}\tau) + f^{*2} \quad (36)$$

which we set equal to $\exp(-2\bar{\Gamma}_{app}\tau)$. In the limit $\tau \to 0$, we then have

$$\bar{\Gamma}_{app} = (1 - f^*)\bar{\Gamma} \quad (37)$$

In line width measurements, we can, therefore, compute f^* from deviations ($\bar{\Gamma} - \bar{\Gamma}_{app}$) in a plot of Γ_{app} vs. $\sin^2(\theta/2)$ where we have taken $\Gamma_{app} \approx \bar{\Gamma}$ at $\sin^2$ large scattering angles. Then, $f^* = (\bar{\Gamma} - \Gamma_{app})/\bar{\Gamma} = \Delta\Gamma/\Gamma$. Similarly, from scattering intensity measurements, we can compute f^* from deviations ($I_{app} - I_s$) in a plot of $1/I_{app}$ vs. $\sin^2(\theta/2)$ where we have taken $I_{app} \approx I_s$ at large scattering angles. Then, f^* from intensity measurements is equal to $(I_{app} - I_s)/I_{app} = \Delta I/I_{app}$. Table IIa shows the effects of dust at 60 and 90° scattering angles for a 23.2 wt % polystyrene solution in *trans*-decalin. The agreement between line width and intensity measurements suggests that we can properly correct for the effect of dust, to the first-order approximation for $\bar{\Gamma}$ and I_s.

At higher concentrations, e.g., at 34.6 wt % polystyrene, if we continue to assume a K^2 dependence for the measured average line width $\bar{\Gamma}$, we note that f^* from intensity and line width measurements agrees at 40 °C but disagrees at 20 °C as shown in Table IIb. The disagreement at 20 °C can be attributed to the dominance and relative decay rates between the hydrodynamic mode and the gel mode. A more detailed analysis is presented in the next paper.

Polymer diffusion in moderately concentrated solutions has been reported by Allen et al.[43] for linear atactic polystyrene ($\bar{M}_w$ = 1.10 × 10^5 and 2.00 × 10^5) in cyclohexane. Figure 11 shows plots of $\bar{D}$ vs. C at 40 °C (hollow squares), 30 °C (hollow triangles), and 20 °C (hollow circles). Again, we should stress the change in the physical meaning of $\bar{D}$ as we change the concentration from dilute to semidilute and concentrated solution regions even though $\bar{\Gamma}$ obeys the K^2 dependence over the entire concentration range. The general feature of $\bar{D}$ vs. C can best

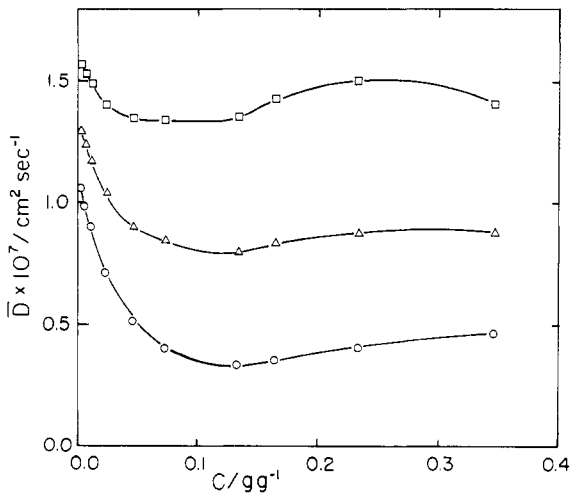

Figure 11. Plots of $\bar{D}$ vs. C at 40 °C (hollow squares), 30 °C (hollow triangles), and 20 °C (hollow circles).

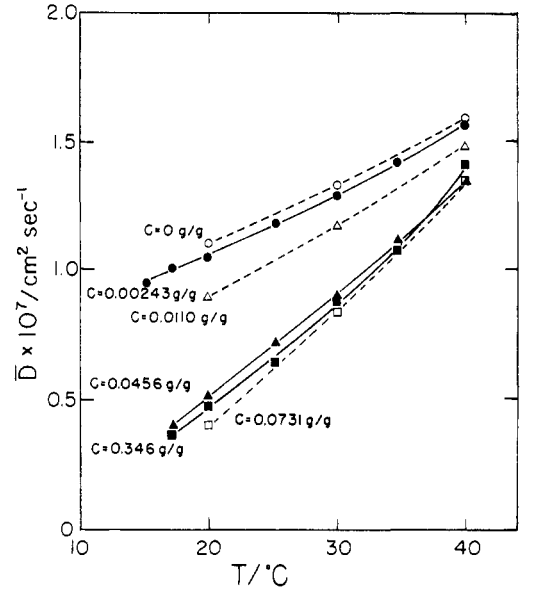

Figure 12. Plots of $\bar{D}$ vs. temperature at different fixed concentrations.

be observed for the curve at 40 °C, i.e., $\bar{D}$ goes through a minimum and then a maximum. For the two curves at lower temperatures, they appear to have a more expanded shape on the concentration axis but would go through a maximum if we could make $\bar{D}$ measurements at high enough concentrations. Similar behavior has been observed by Rehage et al.[44] using macroscopic measurements of the diffusion coefficient. In any case, $\bar{D}$ has been identified to be very close to the macroscopic value.[43] Figure 12 shows plots of $\bar{D}$ vs. temperature at different concentrations. The temperature dependence of $\bar{D}$ leads to small changes in $\bar{r}_h$ with temperature at infinite dilution. Aside from the behavior exhibited in Figure 11, the critical effect is barely visible with the steepest temperature dependence occurring for C = 0.0731 g/g of solution among the concentrations we have investigated. This sharper decrease is in qualitative agreement with the trend observed in Figure 10.

By means of eq 21, we have computed $\bar{f}$ using experimentally determined values of $\bar{M}_w$, $\bar{v}$, C^v $\bar{D}$, and $(\partial\pi/\partial C^v)_{T,P}$. Figure 13 shows plots of $\bar{f}$ vs. concentration at 40 °C (hollow squares), 30 °C (hollow triangles), and 20 °C (hollow circles). Again, it is important to note the graduate transitions in $\bar{f}$ when concentration crosses from the dilute

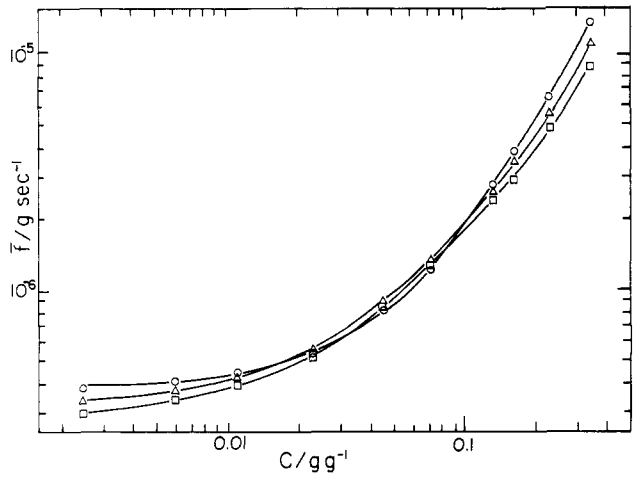

Figure 13. Plots of $\bar{f}$ vs. C at 40 °C (hollow squares), 30 °C (hollow triangles), and 20 °C (hollow circles).

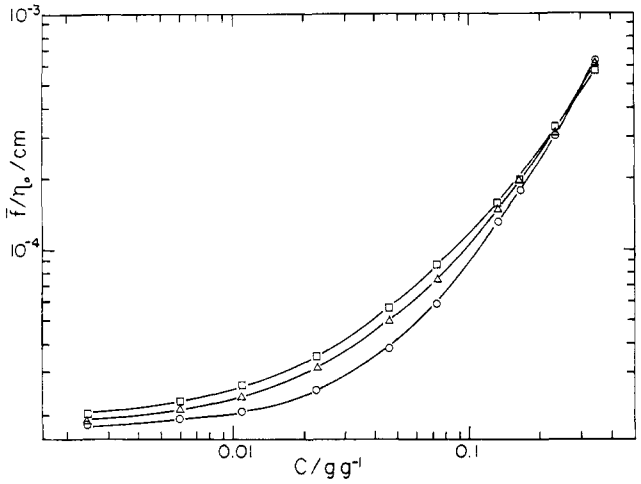

Figure 14. Plots of $\bar{f}/\eta_0$ vs. C at 40 °C (hollow squares), 30 °C (hollow triangles), and 20 °C (hollow circles).

to the semidilute and concentrated solutions. There appears to have been an apparent cross-over effect which can largely be attributed to solvent viscosity effects, as shown in Figure 4 where $\bar{f}/\eta_0$ is plotted against concentration instead of $\bar{f}$ alone. Figure 15 shows plots of $\bar{f}/\eta_0$ vs. T at fixed concentrations. In the dilute solution region, $\bar{f}$ exhibits a slight positive temperature dependence. At higher concentrations, we again observe a steeper temperature-dependent effect. However, $\bar{f}/\eta_0$ varies less strongly with respect to temperature than does $(\partial\pi/\partial C^v)_{T,P}$ in Figure 10 because $\bar{f}$ is proportional to $(\partial\pi/\partial C^v)_{T,P}/\bar{D}$. At very high concentrations, e.g., $C = 0.346$ g/g of solution, we observed a slight negative temperature dependence for $\bar{f}/\eta_0$.

We recall from our earlier discussions that although we have defined the static osmotic compressibility and the dynamical diffusion coefficient, those properties change their meaning as the concentration is increased. For example, at high concentrations where polymer coils overlap, $\bar{D}$ must be related, at least partially, to the collective hydrodynamic mode. The transition from independent translational motions of individual coils to collective motions with a characteristic length related to coil overlap appears to be gradual from the shape of $(\partial\pi/\partial C^v)_{T,P}$, $\bar{D}$, and $\bar{f}/\eta_0$.

In Rayleigh line width spectroscopy, although we observed a K^2 dependence for $\bar{\Gamma}$, the variance changes markedly as a function of concentration. This remarkable increase in the estimated $\mu_2/\bar{\Gamma}^2$ at high concentrations, as

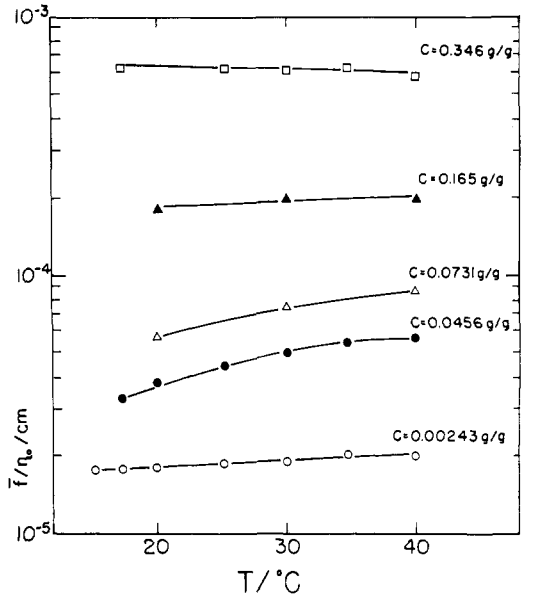

Figure 15. Plots of $\bar{f}/\eta_0$ vs. temperature at different fixed concentrations.

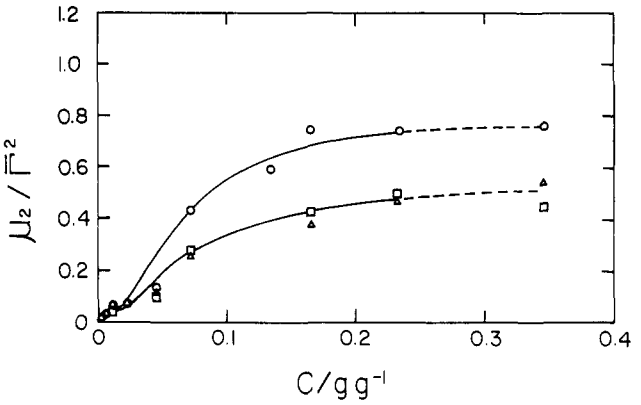

Figure 16. Plots of $\mu_2/\bar{\Gamma}^2$ vs. C at 20 °C (hollow circles), 30 °C (hollow triangles), and 40 °C (hollow squares). Values of μ_2 were obtained by extrapolating those values at fixed order of cumulants to $\tau_{max} = 0$. Such a procedure tends to yield an upper estimate for μ_2.

shown in Figure 16, cannot be attributed to polydispersity effects. At low concentrations in the dilute solution region, the nonzero value of $\mu_2/\bar{\Gamma}^2$ does represent the presence of polydispersity. In fact, a detailed analysis of line widths at infinite dilution will permit a determination of the molecular weight distribution function[41] and at finite concentrations a test of the second virial coefficient k_D. However, at higher concentrations, the value of $\mu_2/\bar{\Gamma}^2$ becomes so large that we suspect the presence of additional decay times. Unfortunately, aside from the moments, the cumulants method does not provide us information on $G(\Gamma)$ itself. Thus, we came to the histogram method of data analysis.

Figure 17 shows a plot of $A\beta|g^{(1)}(\tau)|^2$ and percent deviation (% dev) vs. the delay channel number I for 23.3 wt % polystyrene (NBS 705 standard) in *trans*-decalin at $\theta = 90$ and 20 °C. We define

$$\%\ \text{dev} = 100\left(\frac{Y_m(I) - Y(I)}{Y(I)}\right) \tag{38}$$

where $Y(I)$ is based on eq 30–32 with $G(\Gamma)$ vs. Γ shown in Figure 18. The most important discoveries are that (1) the presence of an additional mode contributes little to $\bar{D}$ but a great deal to $\mu_2/\bar{\Gamma}^2$ because of the distinct bimodal

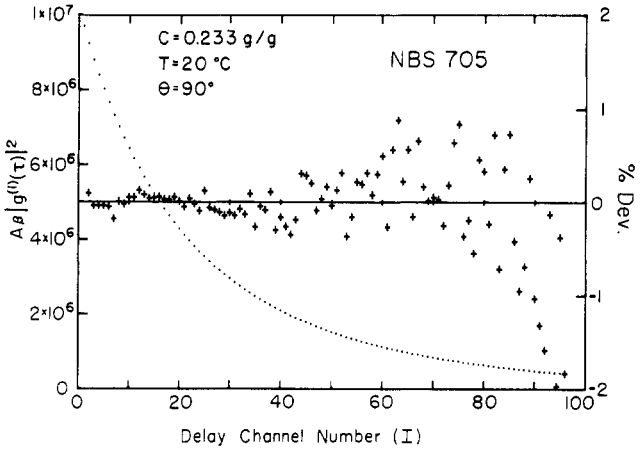

Figure 17. Plots of $A\beta|g^{(1)}(\tau)|^2$ and % dev vs. delay channel number I. $\Delta\tau = 8.2$ μs. % dev = $([Y_m(I) - Y(I)]/Y(I))$ with $Y(I)$ computed according to eq 30–32; $C = 0.233$ g/g of solution.

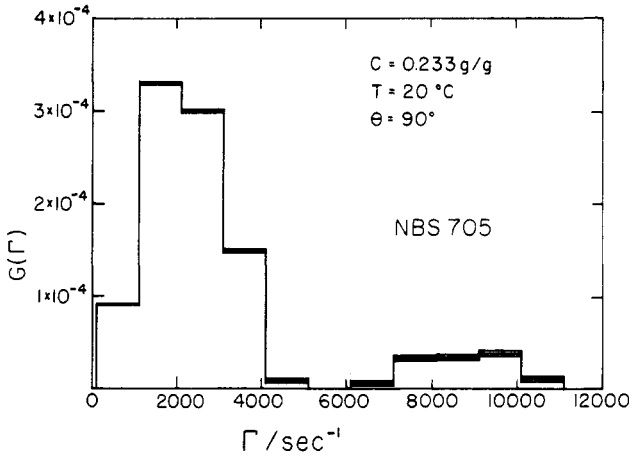

Figure 18. Plot of $G(\Gamma)$ vs. Γ based on a least-squares analysis of data shown in Figure 17.

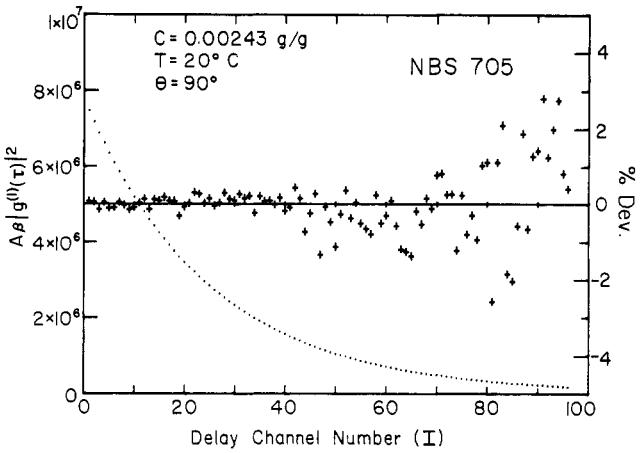

Figure 19. Plot of $A\beta|g^{(1)}(\tau)|^2$ and % dev vs. delay channel number I. $\Delta\tau = 2.65$ μs at $\theta = 90°$ and 20 °C; $C = 0.00243$ g/g of solution.

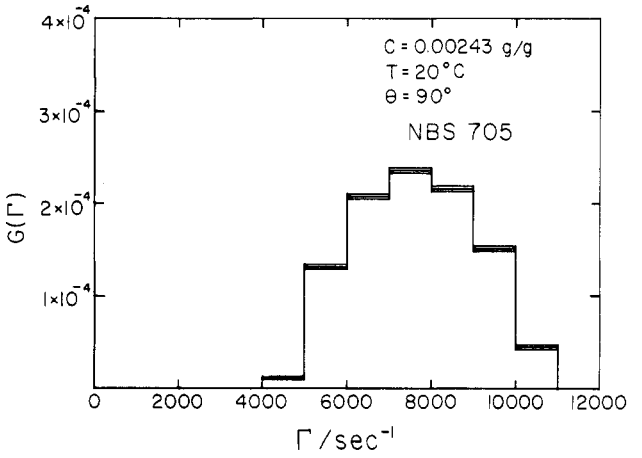

Figure 20. Plot of $G(\Gamma)$ vs. Γ from a dilute polymer solution based on data shown in Figure 19.

nature of $G(\Gamma)$ and (2) the additional mode appears at a higher Γ value. In order to show that the histogram method involves no a priori assumptions, we have also plotted the same solution at the same temperature (20 °C) and the same scattering angle (90°) except at a much lower concentration ($C = 0.00243$ g/g of solution). Figure 19 shows a plot of $A\beta|g^{(1)}(\tau)|^2$ and percent deviation (% dev) vs. channel number I for the dilute solution. We note that both Figures 17 and 19 have been fitted to the statistical error limits from the % dev plots. However, $G(\Gamma)$ in Figure 20 is clearly unimodal. We can identify the faster component with the gel-like mode. A detailed analysis of the line width data using the histogram method is presented in the next article.

Conclusions

Observations at low concentrations have confirmed mainly what is already known in the dilute solution region. The major contributions should come from results in semidilute and concentrated solution regions.

One surprising observation is that $\bar{\Gamma}/K^2$ at fixed concentrations remains essentially constant even at high concentrations (up to 23.3 wt % polystyrene) and the temperature ranges (20–40 °C) investigated. Thus, the major contribution in $\bar{D}$ at moderately concentrated solutions can be identified with macroscopic hydrodynamic values. On the other hand, $\mu_2/\bar{\Gamma}^2$ increases dramatically from near zero to values greater than 0.5 as solution concentration increases from dilute to semidilute and concentrated solution regions. Our histogram analysis has shown the presence of an additional faster mode of motion which is distinct from the macroscopic hydrodynamic mode.

The concentration dependence of osmotic compressibility, diffusion coefficient, or frictional coefficient at different temperatures near the Θ temperature shows gradual transitions from dilute to semidilute and concentrated solutions. Simple power law relations are limiting theoretical forms which need to be modified for application to polymers of finite molecular weight at finite concentrations. Unlike $\bar{D}$, $\bar{f}$ increases monotomically as a function of concentration.

References and Notes

(1) P. G. de Gennes, *Phys. Lett. A*, **38**, 399 (1972); *J. Phys. (Paris)*, **36**, L-55 (1975).
(2) J. des Cloizeaux, *J. Phys. (Paris)*, **36**, 281 (1975).
(3) M. Daoud, J. P. Cotton, B. Farnoux, G. Jannink, G. Sarma, H. Benoit, R. Duplessix, C. Picot, and P. G. de Gennes, *Macromolecules*, **8**, 804 (1975).
(4) M. Daoud and G. Jannink, *J. Phys. (Paris)*, **37**, 973 (1976).
(5) J. P. Cotton, M. Nierlich, F. Boué, M. Daoud, B. Farnoux, G. Jannink, R. Duplessix, and C. Picot, *J. Chem. Phys.*, **65**, 1101 (1976).
(6) P. G. de Gennes, *Macromolecules*, **9**, 587, 594 (1976).
(7) M. Daoud and P. G. de Gennes, *J. Phys. (Paris)*, **38**, 85 (1977).
(8) F. Brochard and P. G. de Gennes, *J. Chem. Phys.*, **67**, 52 (1977).
(9) M. Daoud and G. Jannink, *J. Phys. (Paris)*, **39**, 331 (1977).
(10) M. K. Kosmas and K. F. Freed, *J. Chem. Phys.*, **69**, 3647 (1978).
(11) R. S. Adler and K. F. Freed, *J. Chem. Phys.*, **70**, 3119 (1979).
(12) B. Farnoux, M. Daoud, D. Decker, G. Jannink, and R. Ober, *J. Phys. (Paris)*, **36**, L-35 (1975).
(13) M. Adam and M. Delsanti, *J. Phys. (Paris)*, **37**, 1045 (1976); **38**, L-271 (1977); *Macromolecules*, **10**, 1229 (1977).

(14) E. Dubois-Violette and P. G. de Gennes, *Physics (Long Island City, N.Y.)*, **3**, 181 (1967).
(15) F. Brochard and P. G. de Gennes, *Macromolecules*, **10**, 1157 (1977).
(16) E. Geissler and A. M. Hecht, *J. Phys. (Paris)*, **39**, 955 (1978).
(17) J. P. Munch, S. Candau, J. Herz, and G. Hild, *J. Phys. (Paris)*, **38**, 971 (1977).
(18) E. Geissler and A. M. Hecht, *J. Chem. Phys.*, **65**, 103 (1976).
(19) T. Tanaka, L. O. Hocker, and G. B. Benedek, *J. Chem. Phys.*, **59**, 5151 (1973).
(20) M. Nakata, T. Dobashi, N. Kuwahara, M. Kaneko, and B. Chu, *Phys. Rev. A*, **18**, 2683 (1978).
(21) F. J. Wegner, *Phys. Rev. B*, **5**, 4529 (1972).
(22) D. Patterson, *Macromolecules*, **2**, 672 (1969).
(23) K. S. Soiw, G. Delmas, and D. Patterson, *Macromolecules*, **5**, 29 (1972).
(24) T. Tanaka, S. Ishiwata, and C. Ishimoto, *Phys. Rev. Lett.*, **38**, 771 (1977).
(25) T. Tanaka, *Phys. Rev. A*, **17**, 763 (1978).
(26) H. Yamakawa, *J. Chem. Phys.*, **36**, 2295 (1962).
(27) S. Imai, *J. Chem. Phys.*, **50**, 2116 (1969).
(28) C. W. Pyun and M. Fixman, *J. Chem. Phys.*, **41**, 937 (1964).
(29) S. Imai, *Rep. Prog. Polym. Phys. Jpn.*, **8**, 9 (1965).
(30) H. Yamakawa, A. Aoki, and G. Tanaka, *J. Chem. Phys.*, **45**, 1938 (1966).
(31) M. Kurata, "Modern Industrial Chemistry", Vol. 18, Asakura Publishing Co., Japan, 1975, p 288.
(32) F. C. Chen, A. Yeh, and B. Chu, *J. Chem. Phys.*, **66**, 1290 (1977).
(33) Y. Tsunashima, K. Moro, and B. Chu, *Biopolymers*, **17**, 251 (1978).
(34) J. Ehl, C. Loucheux, C. Reiss, and H. Benoit, *Makromol. Chem.*, **75**, 35 (1964).
(35) P. Outer, C. I. Carr, and B. H. Zimm, *J. Chem. Phys.*, **18**, 830 (1950).
(36) D. E. Koppel, *J. Chem. Phys.*, **57**, 4814 (1972).
(37) Esin Gulari, Erdogan Gulari, Y. Tsunashima, and B. Chu, *J. Chem. Phys.*, **70**, 3965 (1979); B. Chu, Esin Gulari, and Erdogan Gulari, *Phys. Scr.*, **19**, 476 (1979).
(38) M. Nakata, S. Higashida, N. Kuwahara, S. Saeki, and M. Kaneko, *J. Chem. Phys.*, **64**, 1022 (1976).
(39) N. Kuwahara, M. Nakata, and M. Kaneko, *Polymer*, **14**, 415 (1973).
(40) A. Ciferri, *J. Polym. Sci., Part A-2*, 3089 (1964).
(41) Erdogan Gulari, Esin Gulari, Y. Tsunashima and B. Chu, *Polymer*, **20**, 347 (1979).
(42) B. Chu and T. Nose, *Macromolecules*, **12**, 347 (1979).
(43) G. Allen, P. Vasudevan, E. Yvonne Hawkins, and T. A. King, *J. Chem. Soc., Faraday Trans. 2*, **73**, 449 (1977).
(44) G. Rehage, O. Ernst, and J. Fuhrmann, *Discuss. Faraday Soc.*, **49**, 208 (1970).
(45) H. Yamakawa "Modern Theory of Polymer Solutions", Harper and Row, New York, 1971.

Static and Dynamical Properties of Polystyrene in *trans*-Decalin. 2. Correlation Function Profile Analysis by the Histogram Method‡

B. Chu* and T. Nose⁺

Chemistry Department, State University of New York at Stony Brook, Long Island, New York 11794. *Received March 5, 1979*

ABSTRACT: Measured single-clipped net signal photoelectron-count time correlation functions of polystyrene (NBS 705 standard, $\bar{M}_w$ = 179 300) in *trans*-decalin were analyzed by the histogram method. The line width distribution function $G(\Gamma)$ was studied as a function of concentration, temperature, and scattering angle. We observed a fast gellike mode before the overlap concentration C^* was reached. This fast gellike mode is responsible for the anomalous increase in the variance of the line width distribution in dilute solutions (as well as in the semidilute solution region) even though its magnitude can be quite small when $C < C^*$. In the semidilute region, we have identified an upper concentration range (C_g) where the hydrodynamic mode becomes vanishingly small. Finally, decomposition of the line width distribution function permits us to sketch out semiquantitatively the excess integrated intensity behavior of polystyrene in *trans*-decalin from pure solvent to pure polymer.

In a previous communication[1] and a subsequent article,[2] we have examined the static and dynamical properties of a low molecular weight polystyrene sample (NBS 705 standard, $\bar{M}_w$ = 179 300, $\bar{M}_w/\bar{M}_n$ = 1.07) in a Θ solvent, *trans*-decalin, from around the Θ temperature (20.5 °C) to 40 °C over a range of scattering angles (θ) and at different concentrations (C) from dilute solution to the semidilute and concentrated solution regions where polymer coils overlap. We shall refer to the communication[1] and the article[2] as papers 1 and 2 where pertinent references on the scaling theories as developed by de Gennes and others, the experimental methods, and results and discussion based on intensity and the cumulants method of line width analysis have been presented. By using a low molecular weight polystyrene sample in a Θ solvent, we have avoided the complication of mixing the hydrodynamic mode with internal motions of polymer segments and have concentrated our studies in ranges where Kr_g remains relatively small. $K = (4\pi/\lambda)\sin(\theta/2)$ with λ being the wavelength of light in the medium and r_g being the radius of gyration. However, at increasingly higher concentrations even before the concentration reaches the overlap concentration C^* [$=\bar{M}_w/(N_A\rho_s r_g^3)$, with $\bar{M}_w$, ρ_s, and N_A being the weight average molecular weight, the solvent density, and the Avogadro number, respectively], we have observed the variance $\mu_2/\bar{\Gamma}^2$ of the line width distribution function $G(\Gamma)$ reaching values greater than 0.5. For a polydisperse sample, the cumulants method defines the average line width $\bar{\Gamma}$ and the variance $\mu_2/\bar{\Gamma}^2$ as

$$\bar{\Gamma} = \int G(\Gamma)\Gamma \, d\Gamma \quad (1)$$

$$\mu_2 = \int (\Gamma - \bar{\Gamma})^2 G(\Gamma) \, d\Gamma \quad (2)$$

where $G(\Gamma)$ is the normalized line width distribution function and $\int G(\Gamma)\, d\Gamma = 1$. With values of $\mu_2/\bar{\Gamma}^2$ ap-

‡Work supported by the National Science Foundation.
*On leave of absence from Tokyo Institute of Technology, Tokyo, Japan.

0024-9297/79/2212-0599$01.00/0